June 1978, at Jose Abad Santos, Davao del Sur, Mindanao, Philippines. This occurrence, presumably the result of postmortem shell drift, is compatible with known current directions (Fig. 3) and indicates movement of more than 1000 km in a maximum of 138 days, or approximately 7 km per day.

The demonstrated ability of *Nautilus* for rapid, extended movement, combined with postmortem drift of the shell, give the animal and its remains unusual dispersal potential. This corroborates the extensive and often cosmopolitan distribution of Paleozoic and Mesozoic shelled cephalopods. However, final disposition of many *Nautilus* shells, in Palau and elsewhere, is beach stranding. This is unlike the occurrence of many of the fossil forms, particularly ammonoids, which are often preserved as complete shells in what are regarded as moderately deep open water deposits. This points to possible differences in the postmortem buoyancy of some fossil-shelled forms, or perhaps to physicochemical factors that may have inhibited postmortem decay of the body and separation of the shell.

W. BRUCE SAUNDERS
Department of Geology,
Bryn Mawr College,
Bryn Mawr, Pennsylvania 19010
CLAUDE SPINOSA
Department of Geology and Geophysics,
Boise State University,
Boise, Idaho 83725

References and Notes

1. W. B. Saunders, *Natl. Geog. Soc. Res. Rep.*, in press.
2. _____ and C. Spinosa, *Paleobiology* **4**, 349 (1978).
3. B. Carlson and M. V. deGruy, Waikiki Aquarium, Honolulu, caught 74 *Nautilus* at sites B and D (Fig. 1), 20 January to 1 February 1978. At our request, 23 *Nautilus* were tagged and released at site D, including three animals that had been tagged and released at this site during May to July 1977 (Table 1).
4. Means of 33 hydrographic data reports in the Palau region provided by the U.S. National Oceanographic Data Center, Washington, D.C.
5. M. House, in *Organisms and Continents Through Time*, N. F. Hughes, Ed. (Palaeontological Association, London, 1973), pp. 305–317; C. Teichert, *J. Paleontol.* **44**, 1129 (1970); T. Sato and T. Hamada, *Jpn. J. Geol. Geog.* **36**, 149 (1964); H. B. Stenzel, in *Treatise on Invertebrate Paleontology* (Univ. of Kansas Press, Lawrence, 1964), part K, pp. K-59 to K-93.
6. National Geographic Society chart, Islands of the Pacific, scale 1:8,000,000 (1974).
7. The Micronesian Mariculture Demonstration Center and Department of Marine Resources, Koror, Palau, were the bases of operations for our study. We thank M. Madranchar, G. Monaco, J. P. McVey, W. M. Hammer, T. Paulis, and W. Hall for assistance and laboratory and logistical support in Palau; G. Monaco, M. Madranchar, L. Davis, and S. Sokoloff for field assistance; and B. Carlson and M. V. deGruy for independently continuing field aspects of our program in January and February 1978. We also thank J. Maranan and F. Malaki for reporting and returning the Palauan shell from Mindanao. Supported by grants from the National Science Foundation (BMS 75-03393 and DEB 77-14467 to W.B.S.) and by the National Geographic Society and Boise State University.

10 October 1978; revised 26 December 1978

Allan Hills 77005: A New Meteorite Type Found in Antarctica

Abstract. *The unique achondrite ALHA 77005 appears to be related to shergottite meteorites through igneous differentiation and may have affinities with mafic rocks on the earth.*

Meteorite finds in Antarctica during the last several years have greatly increased the number of extraterrestrial samples accessible for scientific study. During the 1977–1978 field season, a joint American-Japanese Antarctic expedition recovered a large number of meteorites from the ice sheet in the vicinity of the Allan Hills, Victoria Land (*1*). One of these meteorites, designated ALHA 77005 (*2*), has proved to be a type of achondrite not previously known. Achondrites are igneous rocks, many of which have basaltic compositions, and thus their origins are understandable in terms of the processes (for example, partial melting and differentiation) which characterize the most abundant terrestrial and lunar igneous rocks. In fact, the generation of basaltic magmas appears to be one of the few characteristics shared by all of the terrestrial planets (*3*). Despite the petrogenetic similarities between achondrites and other igneous rocks, these meteorites commonly display mineralogical and chemical features unique to their respective (presumably asteroidal) parent bodies. However, one class of achondrites, the shergottites, have close similarities with basaltic rocks on the earth (*4*). The new achondrite ALHA 77005 may be related to this class of meteorites.

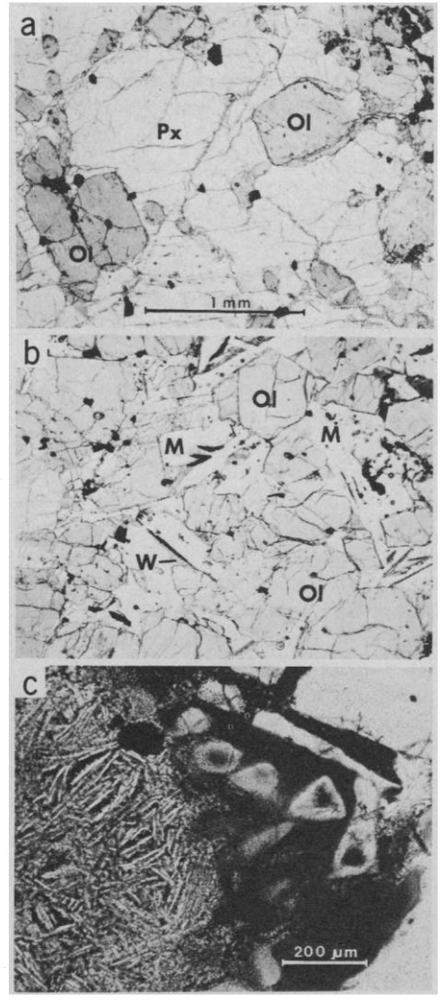

Fig. 1. Textural variations in ALHA 77005 (plane polarized light). (a) Cumulate olivine (*Ol*) and chromite (opaque) crystals poikilitically enclosed by pyroxene (*Px*) in sample 34. (b) Cumulate olivine (*Ol*) with interstitial maskelynite (*M*) and minor ilmenite (opaque) and whitlockite (*W*) in sample 31. Scale as in (a). (c) Patch of vitrophyre containing skeletal and hollow olivine crystals in dark glass.

This meteorite is a rounded stone, weighing 482.5 g, that is partially covered by dark fusion crust (*5*). It is texturally heterogeneous on a centimeter scale. In some areas of the meteorite, euhedral to subhedral olivine and chromite crystals are poikilitically enclosed by pyroxenes (Fig. 1a). The olivines are chemically homogeneous with average composition ~ Fo_{74} (74 mole percent forsterite) (Fig. 2) and have a distinctive brown color. Pyroxenes occur in both low-calcium and high-calcium varieties (Fig. 2). Some pyroxenes exhibit polysynthetic twinning, and all show undulatory extinction and deformation twinning with kink bands. Chromites enclosed by pyroxenes have rims that are slightly more aluminous than the core compositions (arrow *P* in Fig. 3). Minor troilite is associated with olivine. Other areas of the meteorite consist predominantly of subhedral olivine with interstitial maskelynite, titanium-rich chromite, ilmenite, troilite, whitlockite, and less abundant pyroxenes (Fig. 1b). The maskelynite (shocked plagioclase glass) grains are zoned with $An_{54}Ab_{45}Or_1$ (An is anorthite, Ab is albite, and Or is orthoclase) cores and $An_{54}Ab_{53}Or_2$ rims in extreme cases (Fig. 2). Small interstitial pyroxenes may subophitically enclose maskelynite laths; these interstitial grains are slightly more iron-rich than the larger pyroxene grains which enclose olivine and chromite (Fig. 2). Chromites in contact with maskelynite are zoned toward ulvöspinel compositions (arrow *M* in Fig. 3) or have reaction rims of ilmenite, or both. The ilmenite contains 5 to 6 percent MgO (by weight) with minor chromium and negligible Fe^{3+}. The meteorite is relatively

0036-8075/79/0615-1201$00.50/0

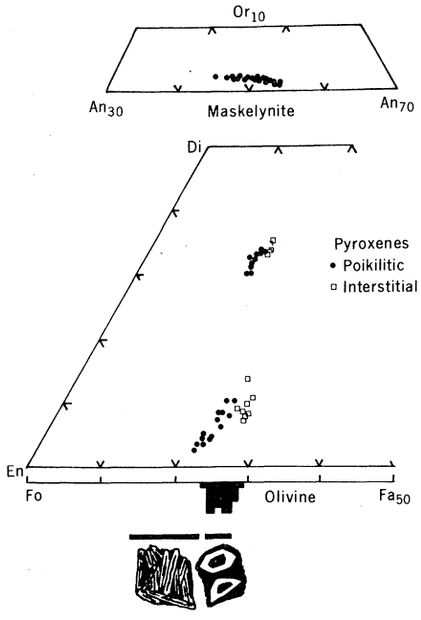

Fig. 2. Mineral compositions (mole percent) determined by microprobe analysis; Fa is fayalite; Di is diopside; other abbreviations in the text. The histogram (bottom center) represents the compositions of cumulus olivines; horizontal bars (at the bottom) are compositional limits of skeletal and hollow olivines in vitrophyre.

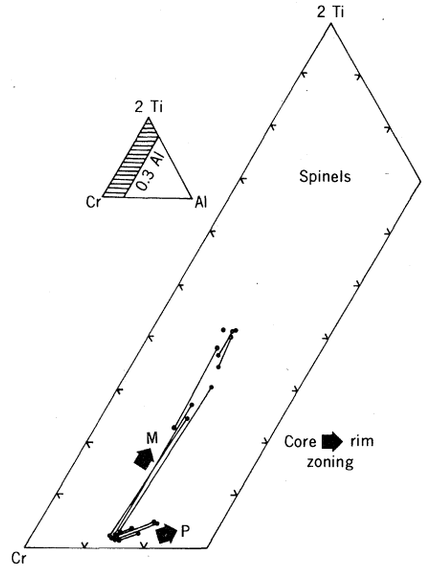

Fig. 3. Compositions of spinels (mole percent) determined by microprobe. Tie-lines connect core and rim compositions in the same grains. Chromites in contact with pyroxene and olivine have slightly aluminous rims (arrow *P*). Chromites in contact with maskelynite (arrow *M*) have titanium-rich rims or are fairly homogeneous grains with high ulvöspinel components.

unaffected by terrestrial alteration, except for isolated areas associated with troilite, which have undergone oxyhydration to form magnetite-maghemite and an FeO(OH) phase, probably akaganeite. Chlorine and chromium (without appreciable nickel) in these alteration products suggest that lawrencite and possibly daubréelite may have been present before alteration. No metal was observed, as previously reported (*5*); however, trace amounts of another phase, probably pentlandite, are associated with troilite.

On the basis of these petrologic observations, the crystallization sequence for ALHA 77005 was as follows: (i) accumulation of olivine and chromite phenocrysts, along with minor troilite which may have wetted settling olivine crystals; (ii) crystallization of low-calcium and high-calcium pyroxenes which poikilitically enclosed cumulus phases; (iii) continued crystallization of intercumulus liquid as plagioclase, minor pyroxene (slightly more iron-rich), ilmenite, and whitlockite; and (iv) late-stage reaction of chromite where it was in contact with interstitial liquid to form titanium-rich chromite and ilmenite, and possible oxyhydration of sulfide minerals and lawrencite to form FeO(OH) minerals.

Transformation of plagioclase to maskelynite and development of deformation twinning and undulatory extinction in pyroxenes are due to postcrystallization shock. In some areas of the meteorite, small patches of melt glass containing skeletal and hollow crystallites of olivine and dendritic chromite grains occur (Fig. 1c). Skeletal crystals have compositions of Fo_{78-86}, and hollow crystals Fo_{73-76} (Fig. 2). These patches of olivine vitrophyre may have formed as impact melts when the meteorite experienced shock. The quenched melt intrudes cracks in grains and has recrystallized and bleached (that is, contact metamorphosed) the immediately adjacent olivine and maskelynite grains.

The petrographic characteristics of ALHA 77005 indicate many similarities with another class of achondrite, the shergottites (*4*). Both meteorite types contain zoned maskelynite with the same compositional ranges, and plagioclases of such intermediate compositions are unknown in other achondrites. The zoned cumulus pyroxenes in shergottites are more iron-rich than pyroxenes in ALHA 77005, but the homogeneous magnesian cores [interpreted in (*4*) to be primocrysts] of shergottite augites ($En_{48}Fs_{20}Wo_{32}$, where En is enstatite, Fs is ferrosilite, and Wo is wollastonite) and pigeonites ($En_{59}Fs_{29}Wo_{12}$) are very similar in composition to the more iron-rich pyroxenes in Fig. 2. In addition, both meteorite types contain whitlockite and ilmenite as accessory minerals.

Although chromite is the spinel phase present in ALHA 77005, titanomagnetite occurs in shergottites. However, the Fe^{3+} contents of some of these chromites ($\sim$ 10 percent by weight of the iron present), calculated from charge balance constraints, suggest that the oxidation state under which ALHA 77005 crystallized may not have been significantly different from that of the shergottites (*6*). A more important difference between these two meteorite types is the degree of silica saturation.

Abundant olivine occurs in ALHA 77005, whereas olivine is absent and a silica polymorph (probably cristobalite) occurs in shergottite mesostasis. The shergottites are clearly more highly differentiated than ALHA 77005 and are consequently richer in iron and silica. It is likely that this new achondrite may represent a cumulate rock formed earlier than the shergottites from the same or a similar parent magma. At some later stage in the differentiation process when shergottites formed, olivine had gone into reaction relationship with the melt. Such a model also explains the difference in spinel compositions, as chromite generally separates early in fractionation sequences. It is not surprising that maskelynite compositions in the two meteorite types are the same despite differences in the degree of differentiation experienced, because plagioclase was probably completely exhausted from the source region at the degrees of partial melting which produced the primary liquids from which these meteorites were derived (*7*).

An alternate interpretation of the origin of ALHA 77005 is that it represents a sample of the (less differentiated) peridotite source region from which shergottite primary liquids were derived. The properties of this achondrite match those predicted for such a source region (*7*); however, if this interpretation is correct, ALHA 77005 cannot have experienced significant partial melting because maskelynite is still present in the residue.

Shock metamorphic features in both meteorite types indicate peak shock pressures near 300 kbar (*8*). The shock metamorphism ages of the two meteorite types ($184 \pm 6 \times 10^6$ years for ALHA 77005 and $164 \pm 12 \times 10^6$ years for Shergotty) determined from rubidium-strontium systematics (*9*) are nearly identical; this result supports the hypothesis that they are related.

If the proposed affiliation with shergottites is correct, ALHA 77005 should ex-

hibit chemical and isotopic features that are similar to the shergottites. Although the major element chemistry will vary as a result of differentiation, minor and trace element ratios should have similar values, provided that the elements considered are not fractionated from each other during igneous processes. The surprisingly young (for a meteorite) radiometric age of crystallization determined for shergottites is $\sim 0.6 \times 10^9$ years (*10*), and a similar value may be obtained for ALHA 77005. If this new achondrite is older, it would suggest that ALHA 77005 represents a relict sample of the source peridotite from which the shergottites formed by later melting. Many of the remarkable similarities between terrestrial basaltic rocks and shergottites [chemistry, oxidation state, and potassium/uranium ratios (*4*)] should extend to ALHA 77005, as this new achondrite may provide an additional sample of the only other body in the solar system known to be similar in composition to the upper mantle of the earth.

HARRY Y. MCSWEEN, JR.
LAWRENCE A. TAYLOR
Department of Geological Sciences, University of Tennessee, Knoxville 37916

EDWARD M. STOLPER
Department of Geological Sciences, Harvard University, Cambridge, Massachusetts 02138

References and Notes

1. Meteorites which fall randomly over the continent are carried toward continental margins by moving ice. The Allan Hills provide a physical barrier for the ice so that meteorites are concentrated in a small area as ice is removed by ablation. Details of the Allan Hills site have been discussed by Y. Yanai, W. A. Cassidy, M. Funaki, and B. P. Glass [*Proc. 9th Lunar Planet. Sci. Conf.* (1978), p. 977].
2. Designations for Antarctic meteorites consist of an abbreviated location name (ALH), a letter designating the search party (A), and a five-digit number beginning with the December year of the austral summer season as the first two digits (77) followed by the meteorite sample number (005).
3. J. A. Wood, *Geotimes* **22**, 29 (1977); J. W. Head, C. A. Wood, T. A. Mutch, *Am. Sci.* **65**, 21 (1977).
4. E. M. Stolper and H. Y. McSween, Jr., *Geochim. Cosmochim. Acta*, in press; J. V. Smith and R. L. Hervig, *Meteoritics*, in press; M. B. Duke, in *Shock Metamorphism of Natural Materials* (Mono, Wilkes-Barre, Pa., 1968). p. 613.
5. B. Mason, *Antarct. Meteorite Newsl.* **1** (No. 2), 9 (1978).
6. T. E. Bunch and K. Keil, *Am. Mineral.* **56**, 146 (1971).
7. E. M. Stolper, H. Y. McSween, Jr., J. F. Hays, *Geochim. Cosmochim. Acta*, in press.
8. P. Stöffler, *Fortschr. Mineral.* **49**, 50 (1972).
9. J. L. Wooden, L. E. Nyquist, D. D. Bogard, B. M. Bansal, H. Wiesmann, C.-Y. Shih, G. A. McKay, *Lunar Planet. Sci.* **10**, 1379 (1979).
10. L. Nyquist, J. Wooden, B. Bansal, H. Wiesmann, G. McKay, D. Bogard, *Geochim. Cosmochim. Acta*, in press.
11. We thank the National Science Foundation and NASA for acquiring and making available these samples. This work was supported by NASA grant NSG-7413 to H.Y.M.

25 January 1979; revised 9 March 1979

Carbon Dioxide in the Ocean Surface: The Homogeneous Buffer Factor

Abstract. *The amount of carbon dioxide that can be dissolved in surface seawater depends at least partially on the homogeneous buffer factor, which is a mathematical function of the chemical equilibrium conditions among the various dissolved inorganic species. Because these equilibria are well known, the homogeneous buffer factor is well known. Natural spatial variations depend very systematically on sea surface temperatures, and do not contribute significantly to uncertainties in the present or future carbon dioxide budget.*

Injection of anthropogenic CO_2 into the atmosphere may cause a serious deterioration of global climate. It is likely that geochemical processes will eventually transfer much of this CO_2 to the oceans. The dissolution of atmospheric CO_2 in surface seawater is enhanced by the oceans' capacity to buffer the associated changes in seawater chemistry. The buffering capacity of seawater depends on the conditions and reactions that control the partitioning of carbon within the oceans. For example, reactions with carbonate minerals may tend to maintain relatively constant carbonate ion concentrations, or metabolic processes may buffer against changing pH conditions. We have chosen to examine the most frequently cited buffering mechanism: the homogeneous reaction of dissolved CO_2 with other dissolved inorganic species in seawater. Estimates of the effectiveness of this mechanism vary widely (*1*). Our calculations, using GEOSECS surface water data from the Atlantic and Pacific oceans, clarify some of these differences and their significance for global CO_2 models.

The homogeneous buffering mechanism is frequently evaluated in terms of the buffer factor (*2*)

$$\frac{dpCO_2/pCO_2}{dTCO_2/TCO_2}$$

where TCO_2 is the total concentration of dissolved inorganic carbon in surface seawater equilibrated with the atmospheric CO_2 partial pressure pCO_2. Because this homogeneous buffer factor excludes any heterogeneous reactions that might affect seawater total alkalinity (TA), it is more accurately defined as

$$B_{hom} = \left(\frac{\partial pCO_2}{\partial TCO_2}\right)_{TA} \times \frac{TCO_2}{pCO_2} \quad (1)$$

The homogeneous buffer factor refers by definition to an equilibrium state, and it can be calculated from the relevant equilibrium relationships. To "measure" B_{hom} in seawater is, in effect, to determine the appropriate equilibrium constants for a particular composition and temperature. Five sets of salinity- and temperature-dependent values for these constants have been published during the last 30 years (*3–8*). We have used them to calculate B_{hom} according to the equation

$$B_{hom} = TCO_2\left\{[H_2CO_3^*] + [CO_3^{2-}] + \frac{\gamma[HCO_3^-] - 4[CO_3^{2-}]^2}{[HCO_3^-] + 4[CO_3^{2-}] + \gamma}\right\}^{-1} \quad (2)$$

where

$$\gamma = \frac{TB(K_B')a_{H^+}}{(K_B' + a_{H^+})^2} \quad (3)$$

and a_{H^+} is the hydrogen ion activity , the brackets denote total single ion plus complex ion concentrations, $[H_2CO_3^*]$ is the sum of the concentrations of dissolved CO_2 and carbonic acid, TB is the total concentration of dissolved borate, and K_B' is the first apparent dissociation constant of boric acid (*9*).

Figure 1a shows that the different sets of constants yield B_{hom} values that agree within 0.5 percent in warm waters and 4 percent in cold waters. The constants of Buch (*3*) and Edmond and Gieskes (*5*) are not consistent with experiments performed as part of the GEOSECS program (*10*). If these two sets of constants are ignored, the maximum difference in Fig. 1a is less than 1 percent throughout the full range of sea surface temperatures.

Figure 1a also shows the maximum range of B_{hom} error that might be associated with published uncertainties in the GEOSECS TCO_2 and TA data (*10, 11*). These margins of error range from about $\pm$ 1 percent in warm waters to $\pm$ 3 percent in cold waters.

Figure 1b shows that natural spatial variations in the ocean mixed layer greatly exceed the analytical margins of error associated with B_{hom}. These spatial variations would seem to explain the broad range of published buffer factor values (*12*). They result primarily from the tendency of the sea surface to remain near equilibrium with atmospheric CO_2 at different temperatures. This conclusion is demonstrated by the curve shown in Fig. 1b, which was calculated

0036-8075/79/0615-1203$00.50/0